JOURNAL OF AIRCRAFT
Vol. 54, No. 4, July–August 2017

Assessing Impact of Epistemic and Technological Uncertainty on Aircraft Subsystem Architectures

Imon Chakraborty* and Dimitri N. Mavris†
Georgia Institute of Technology, Atlanta, Georgia 30332

DOI: 10.2514/1.C034007

The progressive transition from conventional to More Electric aircraft subsystem architectures occurring in the aerospace industry necessitates earlier consideration of subsystem impacts in the design process. Significant challenges arise in this regard due to the unavailability of historical information regarding unconventional subsystem architectures as well as the limited definition of the aircraft that exists during the early design phases. This paper assesses the impact of sources of uncertainty on subsystem architectures using the Integrated Subsystem Sizing and Architecture Assessment Capability, which links subsystem and aircraft sizing and analyses. Uncertainty may arise due to limitations, assumptions, or simplifications in the undertaken modeling approach or due to variations in the assumed or projected technological state-of-the-art. In this work, some of these major sources of uncertainty are identified and propagated into the performance analysis of a selected number of subsystem architectures. Both the gross effect of all identified sources of uncertainty and the relative impacts of individual ones are evaluated. More substantially electrified subsystem architectures are seen to retain a performance advantage even in the presence of epistemic uncertainty and show more significant improvement with improving technological state-of-the-art, most notably that of power electronics, electrical generators, and electric motors.

I. Introduction

THE aircraft subsystems, also known as aircraft equipment systems [1], are necessary for performance, safety, controllability, and comfort. To perform their intended functions, subsystems require power, which is termed secondary or non-propulsive power and is typically provided by the aircraft main engines (in addition to primary or propulsive power). Secondary power is extracted from the gas turbine in two forms [2,3]: 1) pneumatic power, obtained by extracting ("bleeding") hot and pressurized air (called "bleed air") from the gas turbine compressor stages, and 2) mechanical power, obtained by driving a gearbox off the gas turbine shaft. The shaft-power thus obtained may further be converted into two additional forms of power: 1) hydraulic power, obtained by driving a hydraulic pump off the gearbox, and 2) electric power, obtained by driving an electrical generator off the gearbox.

Over several decades, the existing technological state-of-the-art (SOTA) and a general "better the devil you know" philosophy [4] led to the development of a conventional subsystem architecture (Fig. 1, left). In this conventional architecture, the environmental control system (ECS) and ice protection systems (IPS) use pneumatic power, and the actuation functions require hydraulic power, whereas avionics and various cabin loads use electrical power [3]. Such an architecture has, however, reached technology saturation, and currently within the industry, there is great interest in electric solutions for the various aircraft subsystems. The industry's progressive approach has thus far resulted in some in-service More Electric Aircraft (MEA) [5,6], in which some of the subsystems have been electrified, whereas others retain a conventional design. If the trend of increasing electrification continues, an All Electric Aircraft may result in the limit (Fig. 1, right), in which all subsystems are powered electrically. The presence of multiple design solutions for multiple subsystems creates a potentially large combinatorial space of subsystem architectures, and there is naturally significant interest in analyzing such a space to identify high-performing architectures from within it.

The predicted performance from such analyses, if obtained in the early design phases, will be subject to considerable uncertainty. First, there will be epistemic uncertainty (from Greek epistēmē or epistēmikós, meaning "of or relating to knowledge or knowing") arising from limitations, assumptions, or simplifications pertaining to the implemented modeling/analysis approaches as well as from the limited or incomplete knowledge regarding the design that exists during these phases. Second, the predicted performance of subsystem architectures is also affected by the assumed technological SOTA. The SOTA may have to be projected into the future to correspond to an airplane concept's estimated entry-into-service and thus is a source of uncertainty. This is especially true for newer technologies that are on steep development curves, for which predictions of the SOTA for a future date are subject to considerable uncertainty. In this work, the impact of such uncertainties on the performance of some selected subsystem architectures is ascertained by 1) using Integrated Subsystem Sizing and Architecture Assessment Capability (ISSAAC) to simultaneously size the aircraft and subsystems, 2) identifying some of the major sources of epistemic and technological uncertainty, and 3) analyzing their effect on the vehicle performance through a parsimonious modeling approach.

Toward this end, the remainder of this paper is organized as follows. Section II provides an overview of the main modules and underlying approach for ISSAAC. Section III describes in brief the modeling and simulation approach for the relevant subsystems. Section IV assesses the impact of epistemic uncertainty on the predicted performance of certain selected subsystem architectures. This is followed by an evaluation of the impact of technological SOTA on the predicted performance of certain architectures in Sec. V. Finally, Sec. VI concludes the paper and identifies avenues for future work.

II. Overview of Integrated Subsystem Sizing and Architecture Assessment Capability

The main modules of ISSAAC that deal with integrated sizing and analysis for the aircraft and its subsystems are depicted in Fig. 2. For a more detailed description of each of the constituent modules, the interested reader is referred to other works [7,8]. In this paper, the modules are discussed briefly as follows.

Received 5 May 2016; revision received 14 September 2016; accepted for publication 1 October 2016; published online 28 December 2016.

*Research Engineer II, Aerospace Systems Design Laboratory, School of Aerospace Engineering. Member AIAA.

†S.P. Langley Distinguished Regents Professor, Aerospace Systems Design Laboratory, School of Aerospace Engineering. Fellow AIAA.

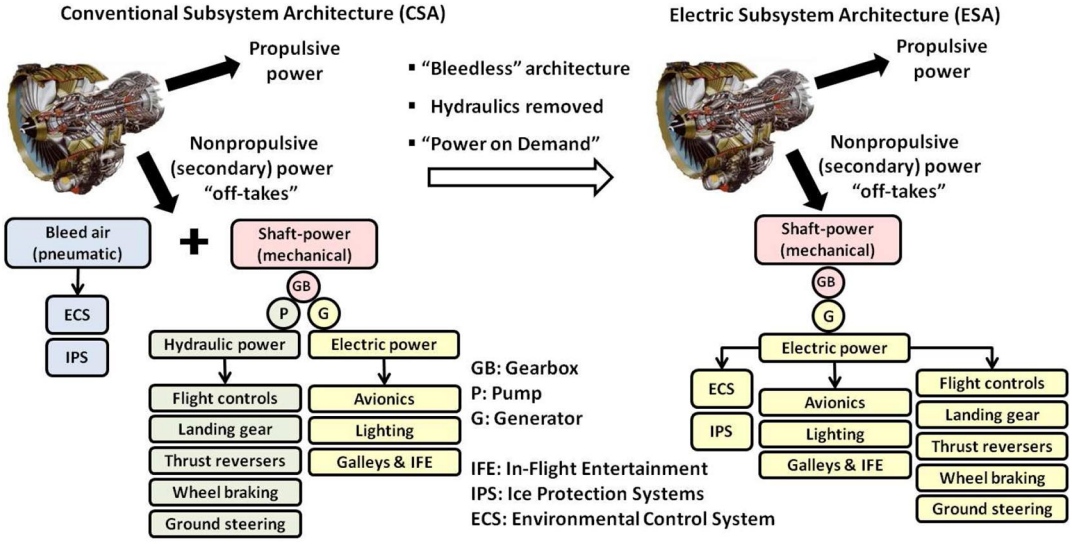

Fig. 1 Secondary power usage of major aircraft subsystems in conventional and All Electric architectures.

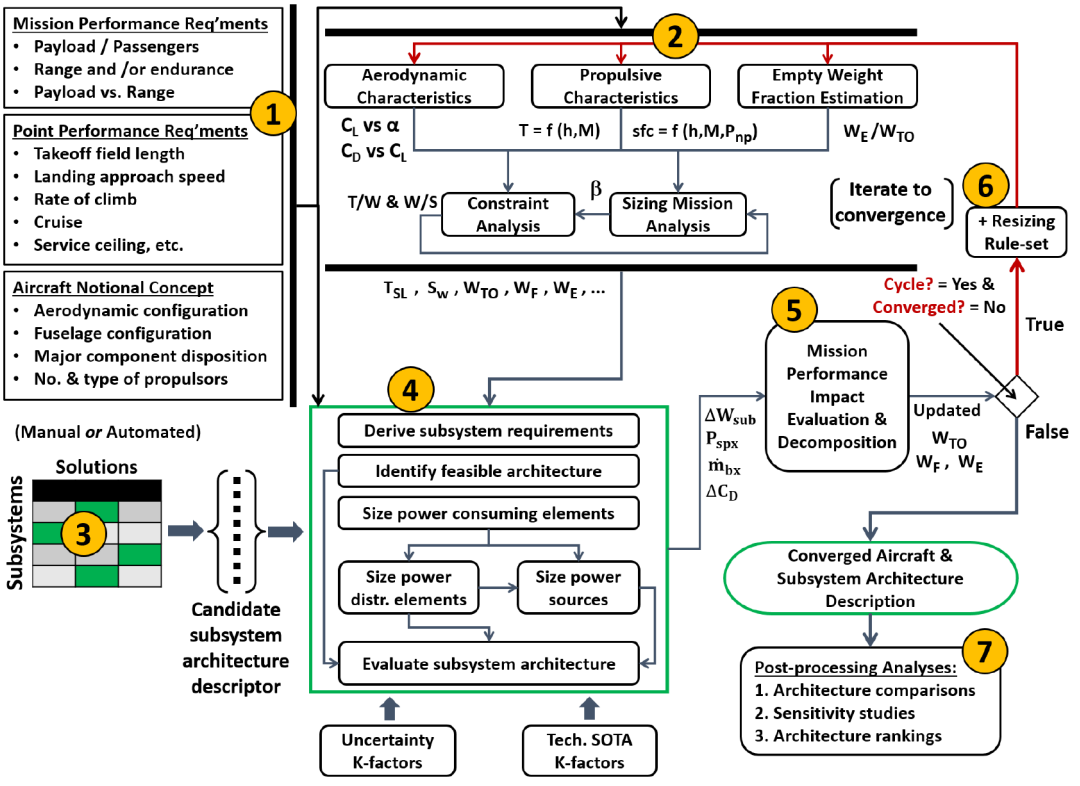

Fig. 2 Main modules of ISSAAC.

A. Definition of Design Requirements

These include the mission performance requirements (e.g., payload-range envelope), the point performance requirements, and the aircraft notional concept. In this paper, aft-tailed tube-and-wing commercial transport designs are considered. Results are presented for three aircraft sizes (described in Appendix A, Table A1): 1) small single-aisle aircraft (SSA), 2) large twin-aisle aircraft (LTA), and 3) very large aircraft (VLA).

B. Traditional Aircraft and Engine Sizing

Here, the goal is to define the aircraft through a geometric scale (represented by wing planform area S_w), a propulsive scale (represented by required sea-level static thrust T_{SL}), and key weights such as takeoff gross weight W_{TO} and empty weight W_e. This is done using the Flight Optimization System (FLOPS) tool developed by NASA Langley Research Center [9] and Numerical Propulsion System Simulation [10] to generate the engine performance characteristics. The weight buildup relationships within FLOPS are based on regressions of historical data and therefore apply to conventional subsystem architectures. Thus, in the first iteration, a conventional subsystem architecture serves as the starting point for the remaining modules.

C. Candidate Subsystem Architecture Descriptor

This provides a qualitative description of the subsystem architecture to be evaluated (e.g., pneumatic versus electric ECS, hydraulic versus electric actuation functions, etc.). The descriptor takes the form shown in Fig. 3. For automated architecture space

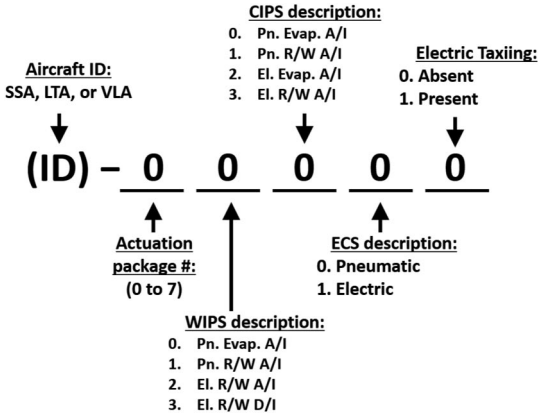

Fig. 3 Naming and numbering scheme for candidate subsystem architecture descriptor.

exploration, descriptors may be obtained from a matrix of alternatives (as shown in Fig. 2). They may also be input manually for the evaluation of a limited number of architectures.

D. Subsystem Architecture Sizing and Evaluation

This module performs the sizing of the major power-consuming elements, power distribution elements, and power sources within the subsystem architecture (a generalized representation of which is shown in Fig. 4a). The modeling approach is described briefly in Sec. III and in greater detail in [7]. The outputs of this module are the difference in weight ΔW_{sub} of the considered architecture relative to a conventional one and the time histories of the architecture's shaft-power requirement $P_{\text{spx}}(t)$, bleed air requirement $\dot{m}_{\text{bx}}(t)$, and direct drag increment $\Delta C_D(t)$. The latter three quantities, which may be time-varying, are computed for each subsystem and for the architecture as a whole. Variation factors or K-factors representing epistemic or technological uncertainty may also be input into this module. These factors are associated with the underlying subsystem parameters and allow the impact of uncertainties to be propagated.

E. Mission Performance Impact Evaluation and Decomposition

This module re-evaluates the impact of the subsystem architecture on the mission fuel requirement using the information generated by the previous modules. As shown in Fig. 4b, the impact is through weight, secondary power requirements, and drag increments. First, the impact of the architecture weight change ΔW_{sub} is computed by linking the computed subsystem weights to the FLOPS mission performance analysis through the appropriate weight override factors [9]. Next, the effects of time-varying shaft-power requirement $P_{\text{spx}}(t)$, bleed air requirement $\dot{m}_{\text{bx}}(t)$, and direct drag increments $\Delta C_D(t)$ are computed from the changes in lift, drag, thrust, and fuel flow caused by these at each point within an invariant mission profile that terminates with a certain (constant) landing fuel reserve. Subject to these assumptions, the additional fuel $\Delta W_f^{(\text{TO})}$ required at takeoff on account of $P_{\text{spx}}(t)$, $\dot{m}_{\text{bx}}(t)$, and $\Delta C_D(t)$ is computed by solving the following equation system backward in time (from landing, $k = n$, to takeoff, $k = 1$), with the intent of computing the takeoff fuel increment $\Delta W_f^{(\text{TO})} = \Delta W_f^{(1)}$:

$$\Delta C_L^{(k)} = \frac{\Delta W^{(k+1)}}{((1/2)\rho V^2)^{(k)} S_w} = \frac{\Delta W_f^{(k+1)}}{((1/2)\rho V^2)^{(k)} S_w} \tag{1a}$$

$$\Delta C_{D_i}^{(k)} = C_{D_i}(C_{L,0}^{(k)} + \Delta C_L^{(k)}) - C_{D_i}(C_{L,0}^{(k)}) \tag{1b}$$

$$\Delta D_{\text{ddl}}^{(k)} = \left(\frac{1}{2}\rho V^2\right)^{(k)} S_w \Delta C_{D_i}^{(k)} \tag{1c}$$

$$\Delta D_{\text{dil}}^{(k)} = \left(\frac{1}{2}\rho V^2\right)^{(k)} S_w \Delta C_{D_0}^{(k)} \tag{1d}$$

$$\Delta D^{(k)} = \Delta D_{\text{ddl}}^{(k)} + \Delta D_{\text{dil}}^{(k)} \tag{1e}$$

$$\Delta T^{(k)} = \Delta D^{(k)} + \Delta W^{(k+1)} \left(\frac{\dot{h}}{V} + \frac{1}{g}\dot{V}\right)^{(k)} \tag{1f}$$

$$T^{(k)} = T_0^{(k)} + \Delta T^{(k)} \tag{1g}$$

$$\Delta \dot{w}_f^{(k)} = \dot{w}_f(T^{(k)}, h^{(k)}, M^{(k)}, P_{\text{spx}}^{(k)}, \dot{m}_{\text{bx}}^{(k)}) - \dot{w}_f(T_0^{(k)}, h^{(k)}, M^{(k)}, 0, 0) \tag{1h}$$

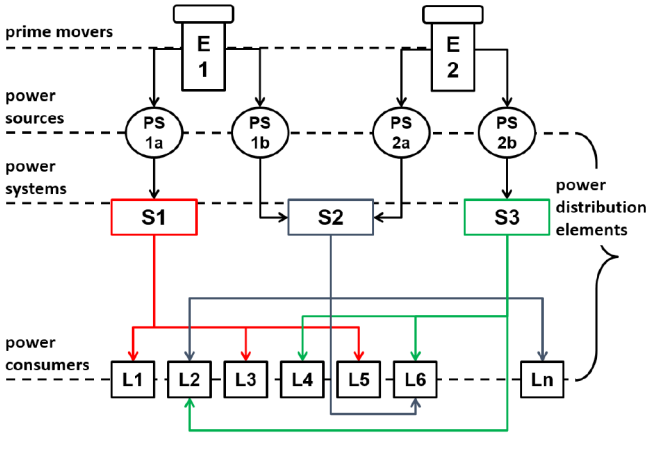

a) Generalized representation of subsystems architecture

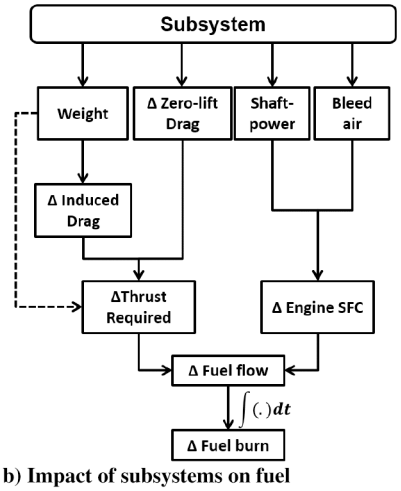

b) Impact of subsystems on fuel consumption (mission-level metric)

Fig. 4 Subsystem architecture representation and impact on fuel consumption.

$$\Delta W^{(k)} = \Delta W^{(k+1)} + \Delta \dot{w}_f^{(k)} \Delta t^{(k)}$$
$$k = k - 1, \quad \text{and} \quad \text{repeat sequence}$$
$$\text{Start point: } k = n - 1, \qquad \Delta W^{(n)} = 0 \tag{1i}$$

The following are the parameters in the preceding equation system: C_L is the lift coefficient; C_{D_i} is the induced drag coefficient; C_{D_0} is the zero-lift drag coefficient; D_{ddl} is the drag dependent on lift; D_{dil} is the drag independent of lift; D is the total drag; T is the thrust; $\dot{w}_f$ is the fuel flow; W is the vehicle gross weight; W_f is the fuel weight; h is the altitude; V is the velocity; M is the Mach number; and $((1/2)\rho V^2)$ is the dynamic pressure. The symbol Δ denotes the increment of a parameter $(\cdot)$ relative to its value $(\cdot)_0$ for an identical reference mission that does not consider the effect of secondary power extraction and drag increments.

F. Resizing of Aircraft and Subsystems

The function of this module is to iteratively resize the aircraft and all subsystems based on certain resizing rules. Subsystem architectures are compared while ensuring that the corresponding aircraft have identical mission performance and point performance capabilities. With regard to the latter, a feasible design may be represented by the wing loading (W_{TO}/S_w) and thrust-to-weight ratio $(T_{\text{SL}}/W_{\text{TO}})$. The assumption that is currently made is that sufficient margin exists between the feasible design point and proximate constraint curves so that any shifts in the latter due to subsystem architecture changes are not sufficient to render the design point infeasible. This assumption results in the following relationships for updating the wing area S_w and engine thrust rating T_{SL}:

$$\Delta S_w = \frac{\Delta W_{\text{TO}}}{(W_{\text{TO}}/S_w)} - \frac{W_{\text{TO}}}{(W_{\text{TO}}/S_w)^2} \Delta\left(\frac{W_{\text{TO}}}{S_w}\right)$$
$$\Delta T_{\text{SL}} = \left(\frac{T_{\text{SL}}}{W_{\text{TO}}}\right) \Delta W_{\text{TO}} + \Delta\left(\frac{T_{\text{SL}}}{W_{\text{TO}}}\right) W_{\text{TO}}$$

Additionally, during resizing, constant stabilizer volume ratios are maintained. This is intended to represent invariant stability and control requirements, subject to the underlying assumption that center-of-gravity shifts on account of subsystem architecture changes do not significantly alter tail moment arms. The iterations terminate when residuals in the gross weight ΔW_{TO}, wing loading $\Delta(W_{\text{TO}}/S_w)$, and thrust-to-weight ratio $\Delta(T_{\text{SL}}/W_{\text{TO}})$ fall below a specified threshold.

G. Post-processing Analyses

This is a customizable module, depending on the type of analysis being performed, and may include a wide range of plots and tabulations as demanded by the analysis. Results presented in this work were post-processed using MATLAB and the statistical analysis tool JMP.

III. Modeling Approach for Subsystems

The subsystems considered within ISSAAC are divided into two groups, as shown in Fig. 5. The modeling and sizing approach for these subsystems is addressed in greater detail in separate works [7,8]. For each subsystem considered, the end goal of the modeling approach is to be able to characterize the subsystem in terms of 1) its weight w_{sub}, as well as the time histories of its 2) shaft-power requirement $P_{\text{spx}}(t)$, if any, 3) bleed air requirement $\dot{m}_b(t)$, if any, and 4) direct drag increment $\Delta C_D(t)$, if any. The subsystems affect fuel consumption through these four avenues, as shown in Fig. 4b. The analysis proceeds by grouping the subsystems into two groups and evaluating them in the following order: 1) power-consuming subsystems, which consume secondary power in pneumatic, hydraulic, or electric form and provide some end functionality to the aircraft; and 2) power generation and distribution subsystems, which are responsible for generation of secondary power, its transformation/regulation, and its distribution to the power consumers.

The connectivity among the subsystem architecture components such as prime movers, power sources, power systems, and power consumers (shown notionally in Fig. 4a) corresponding to a given architecture descriptor is determined automatically by an architecture definition algorithm. This algorithm uses heuristic rules that were identified from inspection of the subsystem architectures of existing conventional aircraft and MEA. The objective of this algorithm is to rapidly determine a feasible architecture connectivity that is equivalent to that seen in existing aircraft from the point of view of redundancy of power sources and systems. The performance of this algorithm was benchmarked by comparing the architecture connectivity predicted by it to the actual connectivity in several existing commercial aircraft [11]. This exercise showed that the heuristic algorithm determined connectivities among subsystem

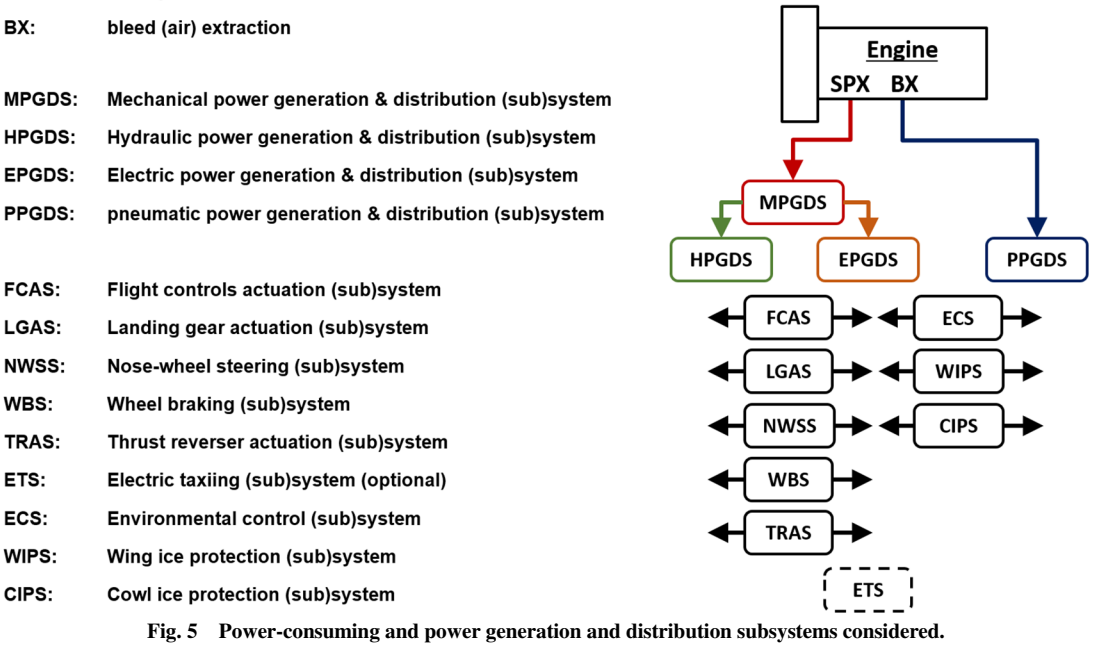

Fig. 5 Power-consuming and power generation and distribution subsystems considered.

architecture components (i.e., between prime movers and power sources, power sources and power systems, and power systems and power consumers, as shown notionally in Fig. 4a) that were equivalent to (or more conservative than) those present in existing commercial aircraft from a redundancy standpoint.

For the flight controls actuation system (FCAS), flight control surfaces are defined relative to the lifting surfaces. For hinged control surfaces such as ailerons, elevators, rudder, and spoilers, the sizing actuation loads are computed using hinge moment coefficients [12] and relevant constraining flight conditions [13,14]. Actuation power requirements are computed using these hinge moment coefficients and assumed duty cycles for the control surfaces [15]. Actuation requirements for the high-lift devices (HLDs) are significantly influenced by actuation mechanism kinematics [16]. For these control surfaces, a relationship between required actuation power and aircraft maximum takeoff mass was obtained using published HLD actuator data for existing aircraft [17–19]. The same approach was followed for the trimmable horizontal stabilizer actuator (THSA), using THSA data for existing aircraft [20]. The actuation requirements for the landing-gear actuation system (LGAS) are computed based on the mass properties of the gear legs and a simplified model of the retraction/extension kinematics [21]. Those for the nose–wheel steering system (NWSS) are computed based on the nose gear's geometry and critical loading conditions that generate maximum steering moments [21,22], an approach that yielded good agreement with published loads from the ELGEAR project [23] for the Airbus A320 aircraft. The wheel braking system (WBS) actuation requirements are derived based on constraining static and dynamic braking cases [14,21,24]. Thrust reverser power requirements are expressed as a linear function of rated sea-level static engine thrust, with the slope and intercept of this relationship estimated based on published figures for the CFM56 engine [25] and the Airbus A380 ETRAS [20]. In each of these cases, the actuator mass is determined based on the actuation load/power that it must be sized to. Because of the presence of multiple actuation functions and multiple actuator designs, a large number of combinations are possible. Instead of considering each, it was assumed that electrification of the actuation functions would occur in a staged or packaged approach through a limited number of actuation packages $P-0, \ldots, P-7$, as shown in Table 1. The successive actuation packages $P-0, \ldots, P-7$ involve electrification of progressively more flight-critical actuation functions.

For the electric taxiing system (ETS) [26], the power requirements and mass addition were assessed in prior work by the authors [27] based on taxiing acceleration/speed requirements and aircraft gross weight. The predicted power showed good agreement with published figures from a collaborative electric taxiing technology demonstration program [26] for the Airbus A320 aircraft. The fuel saved through the use of such a system is computed as a function of total taxiing time.

The ECS power requirement and drag generation is estimated based on 1) a cabin thermal analysis that accounts for internal heat loads and heat transfer between the cabin and the ambient across the cabin wall, and 2) a thermodynamic model of the ECS pack to compute the required mass flow rate of cooling ram air. For electric ECS solutions, mass additions from cabin air compressors, electric motors, and associated power electronics are considered [7], which are driven by the electric pressurization power requirements. The current approach predicted power requirements that compared well with existing estimates for electric pressurization [28] when reduced to a power-per-occupant basis.

For the wing ice protection system (WIPS) and cowl ice protection system (CIPS), the heating requirements are computed based on the surface area to be protected (defined parametrically with respect to the parent surface, i.e., the wing or the nacelle) and the heat flux for a given flight and atmospheric condition [7] computed using only limited geometric information about the aircraft's protected area. Such an approach was shown by other authors [29] to provide acceptable estimates of the IPS power requirements for the Boeing 787 aircraft. The IPS mass is computed using a mass/length figure for pneumatic IPS and a mass/area figure for electrothermal IPS.

For the hydraulic, pneumatic, and electric power generation and distribution systems (HPGDS, PPGDS, and EPGDS respectively), the masses of power distribution elements (hydraulic pipes, pneumatic ducts, and electric cables, respectively) are computed by 1) determining their lengths from the architecture connectivity and the geometric model of the aircraft, and 2) determining the mass per unit length based on consideration of pressure drop, pressure, and voltage drop, respectively. For the HPGDS and EPGDS, power sources (hydraulic pumps and electric generators respectively) are sized through the identification of constraining flight conditions that require the maximum output from these components [7]. Their masses follow from power-to-mass ratios identified from product data sheets.

IV. Effect of Epistemic Uncertainty on Subsystem Architectures

Epistemic uncertainty, as mentioned previously, arises in the current context due to 1) incomplete knowledge and the limited definition of the aircraft that exists in early design phases, and 2) simplifications, assumptions, and limitations inherent to the modeling/analysis approach employed. The latter are necessitated by the need for a computationally tractable analysis using only the available or estimable design characteristics. The epistemic uncertainty directly affects the evaluated subsystem characteristics including weight and secondary power requirements. These subsequently cascade through the remaining analysis modules and ultimately impact the computed mission-level performance of the subsystem architectures. A sensitivity analysis to determine the magnitude of the impact, therefore, represents a significant value addition to a single-point assessment. Such an analysis may be facilitated by the incorporation of variation factors called K-factors associated with internal model parameters that are affected by epistemic uncertainty. There is some latitude regarding the number of such K-factors that are used in the sensitivity analysis. A larger

Table 1 Packaged electrification of actuation functions (FCAS, LGAS, NWSS, WBS, and TRAS)

	Actuation package number (electrification indicated by ✓ or electric actuator type)							
Actuation function	P-0	P-1	P-2	P-3	P-4	P-5	P-6	P-7
TRAS	— —	✓	✓	✓	✓	✓	✓	✓
WBS	— —	✓	✓	✓	✓	✓	✓	✓
LGAS	— —	— —	✓	✓	✓	✓	✓	✓
NWSS	— —	— —	✓	✓	✓	✓	✓	✓
FCAS-HLD	— —	— —	— —	✓	✓	✓	✓	✓
FCAS-Sp[a]	— —	— —	— —	EHA	EMA	EMA	EMA	EMA
FCAS-THSA	— —	— —	— —	— —	✓	✓	✓	✓
FCAS-Prim[b]	— —	— —	— —	— —	— —	H/EHA[c]	EHA	EMA

[a]Sp: spoilers.
[b]Prim: primary flight control surfaces.
[c]Hydraulic actuator and EHA in parallel.

number of K-factors potentially offers greater resolution but results in an expanded sensitivity analysis because more K-factor combinations must be assessed. A parsimonious approach is taken in this work, through which a limited set of K-factors is selected to represent the impact of some major epistemic uncertainty sources, as described in the following section.

A. Identification of Epistemic Uncertainty K-Factors

Considerable uncertainty exists regarding the magnitude of the actuation loads for the flight control surfaces (FCAS). For the primary flight controls, the actuation loads are derived by first estimating the hinge moment coefficients. These depend on the dimensions, locations, and other geometric characteristics (e.g., leading-edge shape) of the control surfaces [12], which are only finalized later in the design process. Similar uncertainty arises in the identification of flight conditions yielding maximum hinge moments [13,14], which requires estimation of flight envelope parameters such as maneuver speed, design cruise speed, and design dive speed as well as certain stability and control coefficients. High-lift device actuating loads are sensitive to flap mechanism kinematics, which vary between aircraft and between manufacturers [16] and are also finalized later in the design process.

Similar uncertainty exists for the remaining actuation functions as well (LGAS, WBS, NWSS, TRAS). For instance, the NWSS sizing actuation load depends on geometric characteristics such as the rake angle and the tire trail, for which only estimates from preliminary design guidelines are available [30]. For the WBS, geometric characteristics of the brakes [31] affect how the deceleration requirements translate to brake actuation requirements. For the LGAS, the retraction loads (and thus the sizing of the retraction actuators) are affected by the retraction mechanism kinematics, which vary between aircraft [32]. They are also naturally affected by the masses and center-of-gravity locations of the gear legs, the braking system (WBS), the steering system (NWSS), and the ETS (if installed), each of which is subject to uncertainty. The TRAS power requirements are also subject to uncertainty because they were inferred from a very limited set of data.

In general, it is impossible to say a priori whether the computed actuation loads will be underpredictions or overpredictions. In fact, it is possible that some actuation loads described previously are underpredicted, whereas others are overpredicted. This can be accounted for by associating a sensitivity factor or K-factor with each and every actuation load or uncertainty source described previously. However, in this work, the overall sensitivity of an architecture's performance to actuation load predictions is assessed by the use of a single K-factor for all the actuation functions. This K-factor $K_{\text{act-loads}}$, which is of a multiplicative nature, is assumed to modify either actuation loads (when these are computed directly) or actuation power requirements.

The actuation power requirements during a mission depend on the activities of the actuation functions. For the LGAS, NWSS, WBS, and TRAS, the activities are well-defined, infrequent, or occur for a fairly small fraction of the overall mission. However, the activities of the primary flight control surfaces and spoilers of the FCAS are not easy to define. The amplitudes of their excursions are dependent upon the required maneuvering authority, the magnitudes of atmospheric disturbances, and the effectiveness of the individual control surfaces. The duration of such activity (as a function of total mission time) is also dependent upon atmospheric conditions. For example, while cruising under calm atmospheric conditions, there may be very little control surface movement, whereas considerable movements may be required under gusty or turbulent conditions. To test the impact of these uncertainties, two additional K-factors are defined for the FCAS. The first, $K_{\text{fcas-acti}}$, multiplies with the assumed activity factor (ratio of time active to mission segment duration). The second, $K_{\text{fcas-amp}}$, multiplies with the peak amplitude of assumed control surface excursions.

For the ECS analysis, the heat transfer rate through the fuselage walls is computed based on an estimate of the total heat transfer area and the effective thermal resistance across the fuselage skin. The trend seen in modern aircraft structures is toward the increased use of composite materials, whose thermal conductivity is typically less than that of metallic skin. At the same time, the contributors to the internal heat load, such as the galley and in-flight entertainment loads, show an increasing trend in modern aircraft. Further, the effects of direct solar radiation incidence on the fuselage and solar radiation through transparencies were not accounted for in the current analysis. The net effect of each of the factors mentioned previously is to increase the net heat load that the ECS has to remove from the cabin to maintain it at the desired temperature. Therefore, the effect of uncertainty in the preceding factors is assessed through the inclusion of a single multiplicative K-factor $K_{\text{ecs-load}}$ (always greater than unity) to multiply the internal heat load seen by the ECS.

For the ice protection systems (WIPS and CIPS), there is uncertainty regarding 1) the estimate of the surface area for which ice protection is required, 2) the estimate of the heat flux required to provide ice protection to a protected surface for a given set of flight and atmospheric conditions, and 3) the assumed overall efficiency of the IPS layout for both pneumatic and electrothermal IPS setups. The ultimate consequence of 1–3 is uncertainty regarding the net heat rate requirement for the WIPS and CIPS. Again, it is not possible to say a priori whether the analysis approach employed will result in an underprediction or an overprediction of the required heat rate. Further, it is possible to underpredict the WIPS loads while overpredicting the CIPS loads, or vice versa. However, the overall impact of uncertainties that influence the computed IPS heat requirement is assessed using a single multiplicative K-factor $K_{\text{ips-load}}$, which is linked to the computed heat rate requirement. It therefore affects the required bleed air mass flow rate (for pneumatic designs) and electric power demand (for electrothermal designs).

For the EPGDS, the total mass of electrical cables is computed by summing contributions from each electrical connection, which are of the form $M_{\text{cbl}}(P_{\text{in}}, L) = \kappa_{\text{inst}}\mathcal{K}_{\text{cbl}}P_{\text{in}}L$. For a given transmitted power P_{in}, uncertainties in the computed mass may arise on account of 1) the mass properties and electrical properties of the conducting material (affecting $\mathcal{K}_{\text{cbl}}$), 2) the cabling length L, whose preliminary estimate does not consider the need to avoid obstacles, and 3) the mass of attachments and fittings, which are not computed directly and are instead represented by the installation factor κ_{inst}. The impact of the preceding uncertainties on computed cabling mass is represented by a multiplicative K-factor $K_{\text{cbl-wt}}$, which multiplies the computed mass of each cable. Following an identical argument, a multiplicative K-factor $K_{\text{duct-wt}}$ is used to multiply the computed mass of pneumatic ducts within the PPGDS to account for mass variations due to the same causes. All K-factors discussed previously are summarized in Table 2. The ranges for each factor were determined through engineering discretion and based on the perceived accuracy of the modeling approaches that were used. The effects of variations of the epistemic uncertainty K-factors on the predicted performance of certain selected subsystem architectures are presented in the following section.

B. Impact of Epistemic Uncertainty K-Factors on Subsystem Architecture Performance

The effects of the sources of epistemic uncertainty identified in the preceding section on the performance of the following four subsystem architectures are analyzed in this work: 1) Arch.-00000: conventional architecture (hydraulic actuation, pneumatic ECS, WIPS, and CIPS); 2) Arch.-70000: fully electrified actuation

Table 2 Summary of epistemic uncertainty K-factors (nominal value for each is 1.00)

K-factor	Subsystem(s) affected	Range
$K_{\text{act-loads}}$	FCAS, LGAS, NWSS, WBS, TRAS	[0.75, 1.25]
$K_{\text{fcas-acti}}$	FCAS	[0.50, 2.00]
$K_{\text{fcas-amp}}$	FCAS	[0.50, 2.00]
$K_{\text{ecs-load}}$	ECS	[1.00, 2.00]
$K_{\text{ips-load}}$	WIPS, CIPS	[0.50, 2.00]
$K_{\text{cbl-wt}}$	EPGDS	[0.75, 1.25]
$K_{\text{duct-wt}}$	PPGDS	[0.75, 1.25]

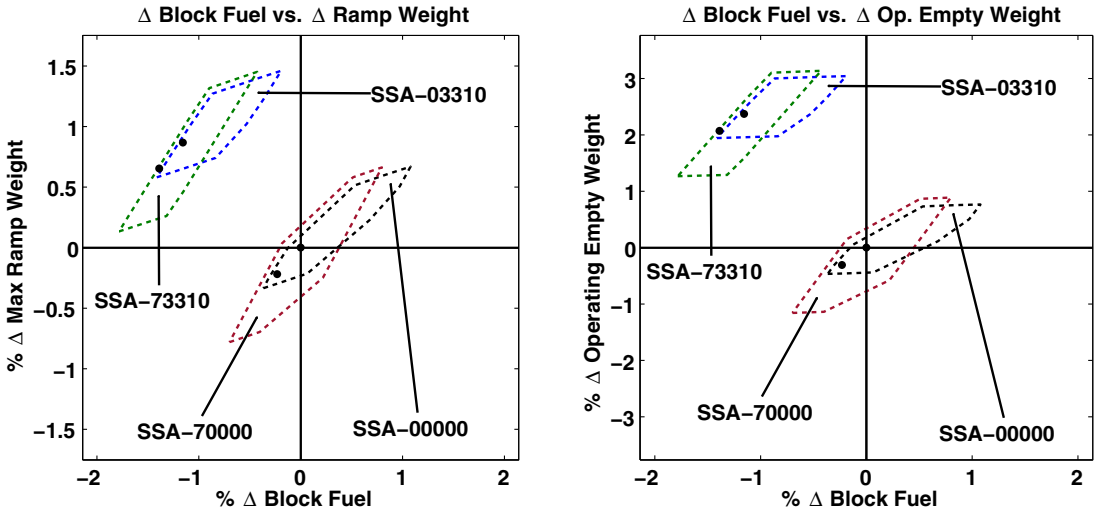

Fig. 6 Gross sensitivity of SSA-00000, SSA-70000, SSA-03310, and SSA-73310 to combined variation of epistemic uncertainty K-factors.

functions, but retaining pneumatics for ECS, WIPS, and CIPS; 3) Arch.-03310: electrified ECS, WIPS, and CIPS, but retaining conventional hydraulic actuation; and 4) Arch.-73310: electrification of all subsystems considered in this work.

For each of these four subsystem architectures, a full-factorial set of K-factor combinations was considered, with each K-factor permitted two levels corresponding to the upper and lower bounds shown in Table 2. This then leads to $2^7 = 128$ case evaluations for each of the four subsystem architectures (thus, 512 architecture evaluations in total). The sensitivity analysis was conducted for the three aircraft sizes (SSA, LTA, and VLA). Because of the observed similarities, only the SSA results are presented in the main text, whereas those for the LTA and VLA are deferred to Appendix B.

Figure 6 indicates the gross sensitivity of these subsystem architectures to the combined variation of all the K-factors listed in Table 2 for the SSA. The block fuel (BF), operating empty weight (OEW), and maximum ramp weight (MRW) are expressed as percentage deltas (%Δ). These are computed relative to the corresponding quantities for the conventional subsystem architecture (-00000) with K-factors set to unity, which therefore occupies the origin by definition. Because lower BF, OEW, and MRW are desirable, the lower-left quadrant is the most desirable, and the upper-right is the most undesirable. The lower-right quadrant is also undesirable because there is a degradation in BF performance. The upper-left quadrant may be acceptable because, despite the increase in aircraft weight, there is a reduction in fuel consumption [33].

The black dots indicate the performance of the four architectures with all K-factors set to unity. The dotted lines represent the boundaries of the convex hulls that contain the predicted performance of the architectures for all other K-factor combinations. Because the original position of the electrified actuation architecture (SSA-70000) is in close proximity to that of the conventional architecture (SSA-00000), the epistemic uncertainty propagation results in significant overlap of the convex hulls corresponding to these two architectures. Thus, it is not possible to guarantee a performance advantage for SSA-70000 relative to SSA-00000 in the presence of epistemic uncertainty. Inspection of the convex hulls for architectures SSA-03310 and SSA-73310 reveals that there are no quadrant crossings for these two architectures due to the variation of the K-factors. Thus, a fuel burn advantage is predicted for these two architectures over the entire range of variation of the K-factors. Between SSA-03310 (hydraulic actuation, electrified ECS, WIPS, and CIPS) and SSA-73310 (additionally, electrified actuation), the sensitivity of the latter's OEW and MRW to K-factor variation is seen to be greater. This is mainly due to the assumption that, with current technology, electric actuators are inferior to hydraulic ones with respect to a load or power per unit mass figure of merit.

Figure 6, however, does not provide information on the relative impacts of the individual K-factors. To assess this, Fig. 7 was generated using the statistical analysis tool JMP. In this plot, the dotted horizontal and vertical reference lines indicate the performance of the considered subsystem architectures with all epistemic uncertainty K-factors at their nominal values (unity). The plotting ranges for BF, OEW, and MRW are identical for all four architectures. The same is true for the x-axis ranges that show the K-factor variations, even though the K-factors themselves have different ranges (Table 2). With these axis settings, the sensitivity of a response (BF, OEW, or MRW) to a particular K-factor is directly indicated by the slope of the corresponding line and by the height of the sensitivity indicator triangles. Because two levels were considered for each K-factor, the sensitivities appear as straight lines. This plot enables the following observations.

1) $K_{\text{act-loads}}$: The sensitivity of BF, MRW, and OEW to this K-factor is greater when actuation functions are electrified (Arch.-7000 and Arch.-73310). This is due to the assumption that electric actuator power-to-mass and force-to-mass ratios are inferior to those of their hydraulic counterparts with current SOTA. Therefore, the same variation in the magnitude of the actuation load resulted in a larger variation in electric actuator mass than in hydraulic actuator mass. For all architectures, the effect of this K-factor is significant because it results in a direct change in surface controls mass that affects the OEW and, through it, the BF.

2) $K_{\text{fcas-amp}}$ and $K_{\text{fcas-acti}}$: The sensitivity of BF, MRW, and OEW to these two K-factors is seen to be marginal. The conclusion that may be drawn is that, although control surface duty cycles affect actuator design significantly (more so for electric actuators [15,34]), the impact on top-level parameters (BF, OEW, and MRW) is not as significant.

3) $K_{\text{ecs-load}}$: For the SSA and LTA, this K-factor does not affect the OEW. For these two aircraft sizes, the increased ECS thermal load could be handled without increasing the cabin mass flow rate, thus not necessitating size/capacity changes for architecture components (for pneumatic ECS, precoolers and pneumatic ducting; for electric ECS, electrical cabling, cabin air compressors, generators, and power electronics). The impact on BF for the SSA and LTA is due to increased ram drag on account of the higher ram air mass flow required to service the higher ECS thermal load. For the VLA, however, the increased ECS thermal load necessitated higher mass flow rates and therefore an increase in the size/capacity (and thus, mass) of the architecture components mentioned previously. The impact on BF is also more significant because it occurs through the combined impact of OEW and the higher secondary power requirements (bleed air for pneumatic ECS, electric power for electric ECS) associated with the higher mass flow rate.

4) $K_{\text{ips-load}}$: This K-factor has a more pronounced effect on conventional pneumatic IPS than on electrothermal IPS for all three aircraft sizes. Variations in IPS heat load clearly affect the bleed air requirement of the pneumatic IPS and the electric power requirement

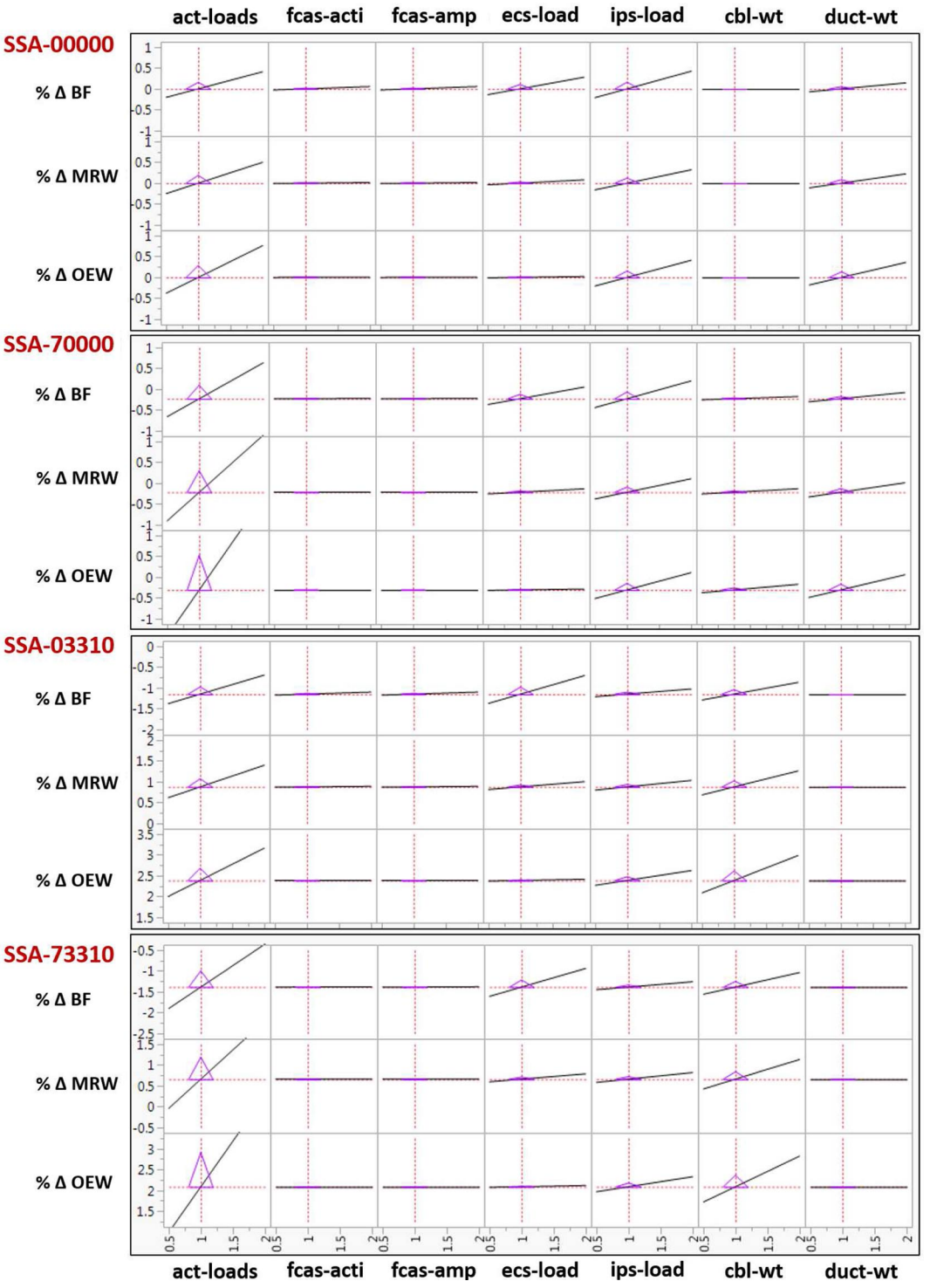

Fig. 7 Impact of individual epistemic uncertainty K-factors on performance of SSA-00000, SSA-70000, SSA-03310, and SSA-73310.

of the electrothermal IPS, but because the IPS operates for a reasonably small fraction of the flight, the observed effect on block fuel is only partially due to the increased off-takes. The majority of the effect is due to the variations in OEW of the aircraft. For pneumatic IPS, this is due to the variations of PPGDS duct and precooler sizes based on the IPS bleed air requirements. For electrothermal IPS, this is due to variations in EPGDS cable and generator masses caused by variations in IPS power requirement.

5) $K_{\text{cbl-wt}}$ and $K_{\text{duct-wt}}$: These two K-factors represent variations in electrical cable and pneumatic duct masses caused by material properties or under/overestimates of their lengths. Because the pneumatic system is invariant between Arch.-00000 and Arch.-70000, so is the sensitivity to $K_{\text{duct-wt}}$ for these two architectures. Because the pneumatic system is removed for Arch.-03310 and Arch.-73310, the effect of this K-factor is naturally nil. The impact of $K_{\text{cbl-wt}}$ increases progressively from Arch.-00000 to Arch.-73310 due to the incorporation of progressively more electrical cabling.

V. Impact of Technological State-of-the-Art on Subsystem Architectures

The predicted architecture performance is influenced by the assumed technological SOTA. Especially for technologies on steep development curves or for which little historical data exist, there is no way to accurately project the SOTA into the future, thus

Table 3 Summary of technological SOTA K-factors

K-factor	Subsystem(s) affected	Settings
$K_{\text{em-sota}}$	Actuation, ECS	{1[a], 2, 3}
$K_{\text{pe-sota}}$	Actuation, ECS, EPGDS	{1[a], 2, 3}
$K_{\text{cac-sota}}$	ECS	{1[a], 2, 3}
$K_{\text{gen-sota}}$	EPGDS	{1[a], 2, 3}
$K_{\text{apu-start}}$	EPGDS	{0[a], 1}

[a]Nominal setting.

resulting in technological SOTA uncertainty. The effect of such uncertainty on the predicted performance of subsystem architectures is assessed by judiciously associating technology K-factors only to architecture components that may see fairly rapid development. The selection of the K-factors is discussed in the following section.

A. Identification of Technological State-of-the-Art K-Factors

As mentioned previously, electric actuators for the actuation functions (FCAS, LGAS, NWSS, WBS, and TRAS) are assumed to be inferior to conventional hydraulic ones with respect to a load or power per unit mass figure of merit with current SOTA. However, it may be improper or misleading to associate a technology K-factor directly to such a figure of merit because not all actuator subcomponents are likely to see equally significant technology advancements. For instance, for electrohydrostatic actuation, the designs of hydraulic components such as pumps and hydraulic cylinders have already reached a high degree of refinement. For electromechanical actuation, the same is true for the designs of mechanical components such as gearboxes and ballscrews. The most significant mass reductions for electric actuators will most likely stem primarily from improved power-to-mass ratios of motors and power electronics. Therefore, it is more logical to associate technology K-factors with these. Here, this is done by representing the actuator mass M_{act} generically as

$$M_{\text{act}} = \frac{\mathcal{X}_0}{(\mathcal{X}_0/M)} + \frac{P_m^{\max}}{\eta_m}\left\{\frac{1}{(P/M)_{\text{em}}}\left(\frac{1}{K_{\text{em-sota}}} - 1\right) + \frac{1}{\eta_{\text{em}}\eta_{\text{pe}}(P/M)_{\text{pe}}}\left(\frac{1}{K_{\text{pe-sota}}} - 1\right)\right\} \tag{2}$$

where $\mathcal{X}_0$ may represent stall load for a linear actuator, maximum output moment $\mathcal{M}_0$ of a rotary actuator, or maximum shaft-power output of a power drive unit (PDU). The corresponding figure of merit $(\mathcal{X}_0/M)$ of the actuator may be identified by reference to specifications of existing actuators of that particular type (Appendix A, Table A2). In the second term of Eq. (2), $P_m^{\max}$ is the maximum mechanical power output of an electric actuator; η_m is the overall efficiency of all hydraulic or mechanical components; $(P/M)_{\text{em}}$ and $(P/M)_{\text{pe}}$ are the power-to-mass ratios of electric motors and power electronics, respectively; and η_{em} and η_{pe} are their corresponding overall efficiencies. The entire second term is neglected for conventional hydraulic actuators.

The representation of Eq. (2) allows the impact of improving technology specifically for electric motors and power electronics to be modeled using the technology K-factors $K_{\text{em-sota}}$ and $K_{\text{pe-sota}}$, respectively. Within More Electric subsystem architectures, motors are not limited merely to electric actuators but also extend to other subsystems such as electric ECS, where they drive the cabin air compressor (CACs). Many considerations go into the selection of the type of motor for a particular application, and the information available in the early design phases may be insufficient to make this determination. Further, improvements in power-to-mass ratio may not be of the same magnitude for all motor types. The same arguments apply to the design of power electronics and power conversion equipment, which will be pervasive within MEA architectures [35]. In the absence of this information, the K-factors $K_{\text{em-sota}}$ and $K_{\text{pe-sota}}$ are used "across the board" to represent technology improvement for all the subsystems considered.

The electrification of the ECS requires the incorporation of significant hardware (thus significant mass), part of which comes from the mass of the CACs. Therefore, the K-factor $K_{\text{cac-sota}}$ is applied to assess the effect of improvements in technological SOTA for this component. It is not clear whether improvements in the power-to-mass ratio of CACs can be of the same magnitude as improvements for motors and power electronics. However, similar ranges were set for $K_{\text{cac-sota}}$ as for $K_{\text{em-sota}}$ and $K_{\text{pe-sota}}$.

As the required power generation capability increases with progressively greater electrification of the major aircraft subsystems, the mass of the generators (engine-driven and APU-driven) also increases. Therefore, improvements in the technological SOTA (power-to-mass ratio) of generators would clearly have an effect on the net addition of mass to the EPGDS. This impact is modeled using the K-factor $K_{\text{gen-sota}}$.

A final K-factor $K_{\text{apu-start}}$ is used to model the effect of factoring in the power generation capacity of the APU generators into the sizing of the engine-driven generators. Therefore, this is not a technology K-factor in the strict sense of the word because no improvements in APU technology are being modeled using it. Instead, a setting of $K_{\text{apu-start}} = 0$ simply indicates that APU generator capacity cannot be factored into the sizing of the EPGDS, whereas $K_{\text{apu-start}} = 1$

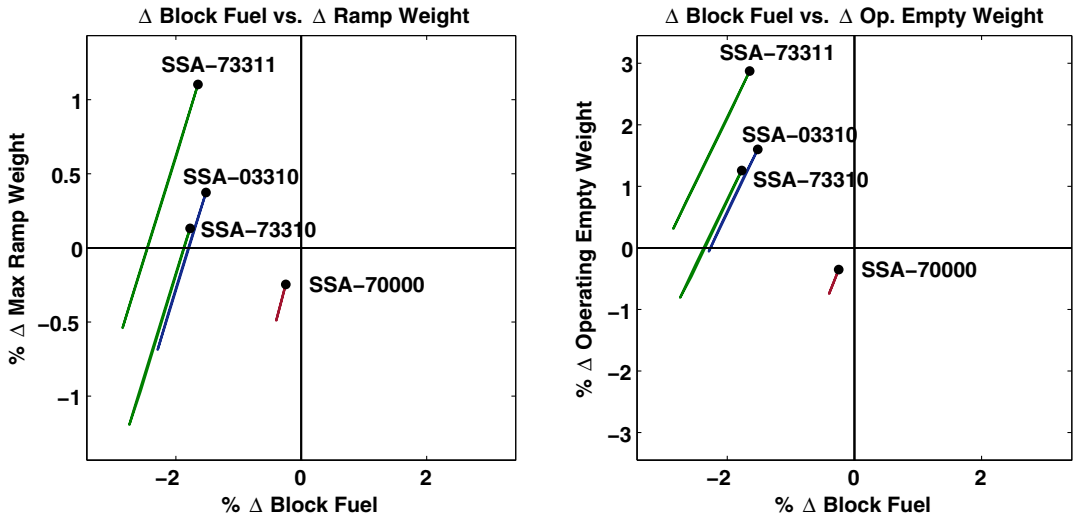

Fig. 8 Gross sensitivity of SSA-70000, SSA-03310, SSA-73310, and SSA-73311 to technological state-of-the-art.

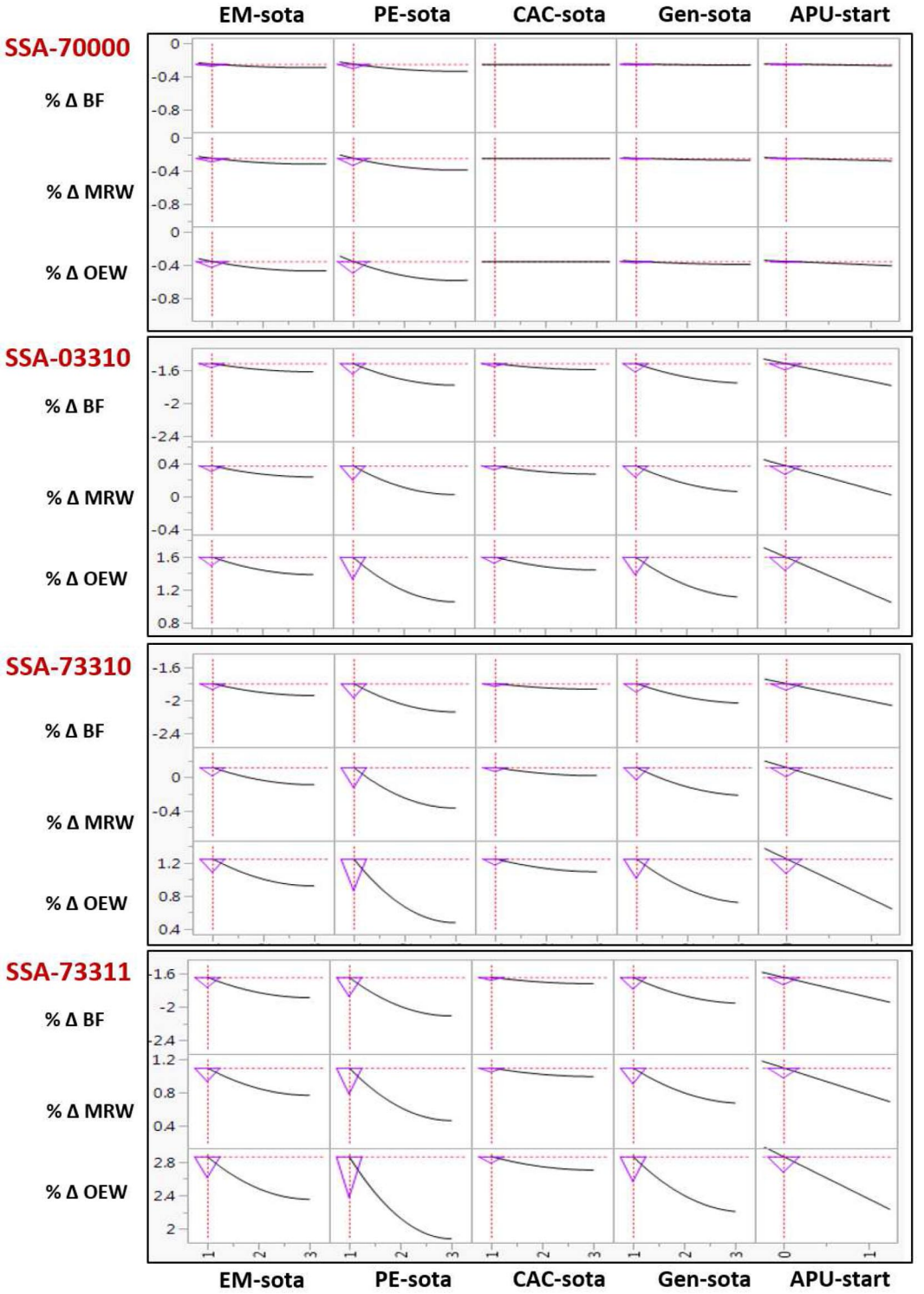

Fig. 9 Impact of individual technological SOTA K-factors on performance of SSA-70000, SSA-03310, SSA-73310, and SSA-73311.

assumes that the engine-driven generator ratings can be downsized based on the availability of the APU generation capacity in contingency/failure scenarios. The impact of variations in the identified technological SOTA K-factors on the performance of a number of selected subsystem architectures is presented in the following section.

B. Impact of Technological State-of-the-Art K-Factors on Architecture Performance

The impacts of the technological SOTA K-factors identified in the previous section on the performance of the following subsystem architectures are assessed in this work: 1) Arch.-70000: fully electrified actuation functions, but retaining pneumatics for ECS, WIPS, and CIPS; 2) Arch.-03310: electrified ECS, WIPS, and CIPS, but retaining conventional hydraulic actuation; 3) Arch.-73310: electrification of all subsystems considered in this work, ETS not installed; and 4) Arch.-73311: electrification of all subsystems considered in this work, ETS installed.

For each of these architectures, a full-factorial set of technological SOTA K-factors was considered, with the K-factors taking the discrete values summarized in Table 3. This results in $3^4 \times 2 = 162$ case evaluations for each of the four subsystem

architectures (thus, 648 architecture evaluations in total). For each K-factor other than $K_{\text{apu-start}}$, the nominal setting of $K_{(.)} = 1$ indicates current technological SOTA (summarized in Appendix A, Table A2), whereas settings $K_{(.)} = 2$ and $K_{(.)} = 3$ indicate twofold and threefold improvement, respectively, in the SOTA. For $K_{\text{apu-start}}$, the nominal setting is $K_{\text{apu-start}} = 0$. The sensitivity analysis was conducted for the SSA, LTA, and VLA. Because of similarities in the observed sensitivities, only the SSA results are presented in the main text, whereas those for the LTA and VLA are deferred to Appendix C.

The overall sensitivity of each of the preceding architectures to the technology K-factors is shown in Fig. 8. Here, too, the BF, OEW, and MRW are expressed as percentage deltas (%Δ) computed relative to the conventional subsystem architecture (-00000) with all technological SOTA K-factors at their nominal settings. The marker dots represent each considered architecture's performance with all technological SOTA K-factors at their nominal settings. The lines emanating from the markers indicate the improvement in architecture performance with improving technological SOTA. The magnitude of predicted improvement is higher for architectures with more substantial electrification (in which motors, power electronics, CACs, and generators account for a higher percentage of the OEW). By this logic, the improvement is most significant for Arch.-73311 (all considered subsystems electrified, ETS installed).

To assess the impacts of the individual technology K-factors (which cannot be inferred from Fig. 8), the JMP tool was used to generate Fig. 9. The dotted vertical and horizontal reference lines show the performance of the architectures considered with all K-factors at their nominal settings ($K_{\text{em-sota}} = K_{\text{pe-sota}} = K_{\text{cac-sota}} = K_{\text{gen-sota}} = 1$ and $K_{\text{apu-start}} = 0$). The plotting ranges for BF, OEW, and MRW are identical for all four architectures. Therefore, the slopes of the curves indicate the sensitivity of a response (BF, OEW, or MRW) to a particular K-factor. The height of the sensitivity indicator triangles indicate the magnitude of the partial derivative of the metrics BF, MRW, and OEW with respect to each K-factor, computed at the nominal K-factor settings. For K-factors other than $K_{\text{apu-start}}$, the curvature indicates diminishing returns with continuing improvement in the technology SOTA, as the contribution of the corresponding components toward overall architecture mass becomes less prominent. The following observations may be made regarding the effects that the technology K-factors have on each of the architectures analyzed.

1) $K_{\text{em-sota}}$: The effect of motor power-to-mass ratio increases as the total contribution of motors to OEW increases. Therefore, it is significant for Arch.-73310, where electric motors exist for all actuation functions as well as to drive the ECS CACs. The effect on Arch.-73311 is greater still, due to additional presence of high power-rating electric motors for the ETS.

2) $K_{\text{pe-sota}}$: The effect of power electronics power-to-mass ratio is the most significant and increases with the proliferation of power electronic components into the subsystem architecture. For Arch.-70000, these include the power converters for the actuators as well as the auto-transformer rectifier units (ATRUs), which convert ac power to dc power. The effect is greater for Arch.-03310 due to the high rating of the CAC power electronics and the increased rating of the ATRUs. The effect is greater still for Arch.-73310 because it combines both electric actuation and electric ECS. Finally, the effect is greatest for Arch.-73311 due to addition of power electronic components for the ETS.

3) $K_{\text{cac-sota}}$: The effect of CAC power-to-mass ratio is less pronounced than that of motor and power electronics power-to-mass ratio. It is also noteworthy that a threefold increase in the SOTA of a mechanical component such as a compressor may not be feasible.

4) $K_{\text{gen-sota}}$: The effect of generator power-to-mass ratio is significant and increases with the required total capacity of the EPGDS. Thus, it is highest for Arch.-73311 (all considered subsystems electrified, ETS installed) due to the significantly higher capacities of both the engine-driven and APU generators.

5) $K_{\text{apu-start}}$: Factoring in the power generation capacity of the APU generators allows the main engine generators to be sized to a lower power rating, thus saving weight. The weight savings is directly related to the power rating of the APU generators and is the greatest for architectures in which the ECS is electric and/or an ETS is installed. However, other practical considerations may also determine whether it is feasible to consider the APU generator capacity while sizing the main engine generators. First, the APU restart envelope would have to extend over the entire flight envelope. Second, it may no longer be possible to dispatch the airplane with an inoperative APU generator.

VI. Conclusions

This paper assessed the impact of epistemic uncertainty and varying technological state-of-the-art on the performance of a selected number of aircraft subsystem architectures. Such an assessment is significant especially for novel architectures, where subsystem impacts must be considered more thoroughly in the earlier phases of design. The impact of uncertainty was assessed using the Integrated Subsystem Sizing and Architecture Assessment Capability (ISSAAC), which links the sizing of the aircraft subsystems to traditional aircraft and engine sizing. Many of the underlying sizing methods rely on first-order physical models, and tractable analysis of multiple subsystem architectures with only the limited information and aircraft definition available in early design phases necessitates certain simplifying assumptions and estimates. This, along with the scarcity or absence of historical data for the unconventional subsystem architectures being considered, results in epistemic uncertainty and technology state-of-the-art assumptions having a significant impact on predicted architecture performance. The impact of major sources of epistemic uncertainty on the sizing and performance of the considered subsystems was modeled using a parsimonious selection of K-factors. A sensitivity study in which these K-factors were varied revealed that more substantially electrified architectures retained an advantage relative to a conventional architecture even in presence of uncertainty. Uncertainties in the actuation loads, environmental control system thermal loads, and ice protection system heating requirements were seen to have prominent impacts, whereas uncertainties in the amplitudes and activities of flight control surfaces did not significantly affect the top-level metrics considered. The impact of technology improvements was assessed using a set of K-factors that were associated with the technological state-of-the-art of architecture components present in More Electric subsystem architectures. This sensitivity analysis showed that more substantially electrified subsystem architectures showed the greatest improvement. The overall improvements were driven to the greatest extent by improving power-to-mass ratio of power electronics, electrical generators, and electric motors. Factoring the APU generator's capacity into the sizing of the engine-driven generators also has an impact on electrified architectures; however, other operational considerations may ultimately determine the feasibility of such a solution. It should be noted that, although the impacts of epistemic uncertainty and technological state-of-the-art on analyzed metrics such as block fuel, operating empty weight, and maximum ramp weight are important, additional considerations such as cost, reliability, and maintenance requirements also contribute toward the overall viability of subsystem architectures. Assessment of these factors is currently beyond the capability of the demonstrated approach.

Possibilities for future work along this avenue include 1) further validation of the current modeling, sizing, and analysis approaches for the subsystems, 2) systematic identification of additional sources of uncertainty affecting subsystem architecture performance, and 3) expanded sensitivity analyses for a larger number of subsystem architectures, with a greater number of K-factors assuming a larger number of values. Such expanded analyses will generate additional insight regarding the magnitude and the nature of the impact of sources of uncertainty.

Appendix A: Aircraft Baselines and Technological State-of-the-Art

Table A1 Data summary for SSA, LTA, and VLA baselines (with conventional subsystems architecture)

Aircraft data	SSA	LTA	VLA
Passenger capacity	170	396	852
Design range, n mile	3000	7800	8200
Cruise Mach number	0.785	0.84	0.85
Maximum ramp weight, lb	175,130	746,610	1,270,000
Sea-level static thrust, lbf	$2 \times 26,244$	$2 \times 114,220$	$4 \times 69,872$
Wing planform area, ft^2	1347	4695	9111
Wingspan, ft	114.8	201.8	266.4
Wing taper ratio	0.24	0.15	0.21
Wing 1/4-chord sweep, deg	25	31.6	30
Horizontal tail (HT) planform area, ft^2	305	1089	2212
HT aspect ratio	5.47	4.50	4.49
HT taper ratio	0.37	0.30	0.39
HT 1/4-chord sweep, deg	30	35	35
VT planform area, ft^2	231	562	1316
VT aspect ratio	1.80	1.60	1.74
VT taper ratio	0.30	0.29	0.39
VT 1/4-chord sweep, deg	30	35	37
Fuselage length, ft	123.3	239.8	230.9
Fuselage maximum width, ft	12.9	20.3	23.4
Fuselage maximum height, ft	12.9	20.3	27.9

Table A2 Assumed figures of merit or technological SOTA for various subsystem architecture components

Actuator/component	$(\mathcal{X}_0/M)$ or (P/M)	Source
Electrohydrostatic actuator (EHA)	2.2 kN/kg	[5]
Electromechanical actuator (EMA)	2.4 kN/kg	[36]
Hydraulic power control unit	3.8 kN/kg	[5]
Hydraulic power drive unit	4.5 kW/kg	[17,37]
Stabilizer trim hydraulic motor	2.4 kW/kg	[38]
Electric motor	1.4 kW/kg	— —
Power electronics	2.0 kW/kg	[39,40]
Cabin air compressors	2.5 kW/kg	— —
Electric generators	2.8 kVA/kg	[39,41]

Appendix B: Sensitivity to Epistemic Uncertainty (LTA and VLA)

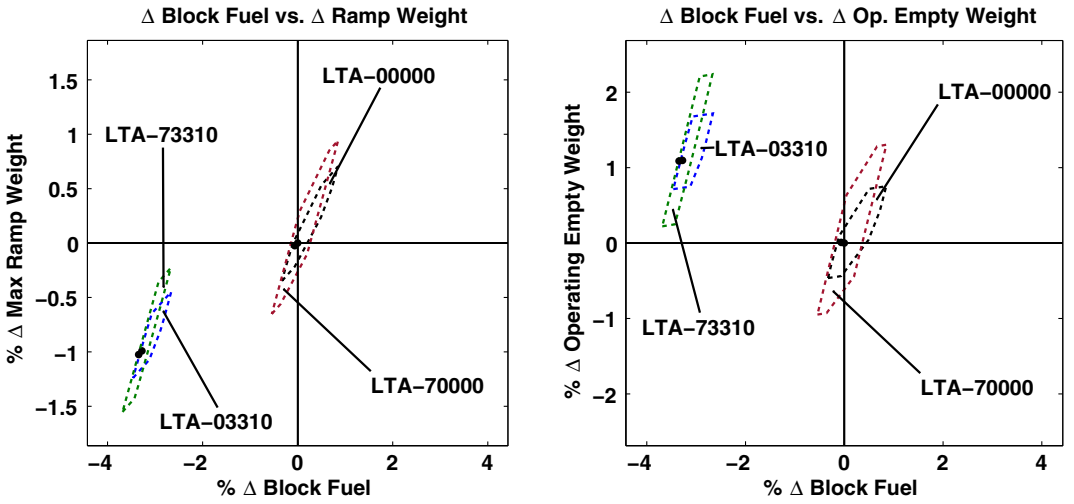

Fig. B1 Gross sensitivity of LTA-00000, LTA-70000, LTA-03310, and LTA-73310 to combined variation of epistemic uncertainty K-factors.

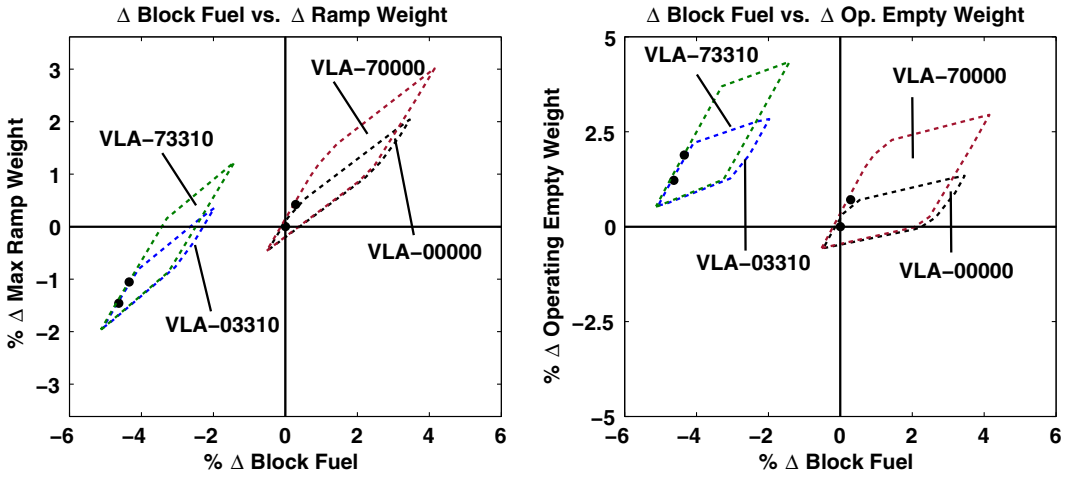

Fig. B2 Gross sensitivity of VLA-00000, VLA-70000, VLA-03310, and VLA-73310 to combined variation of epistemic uncertainty K-factors.

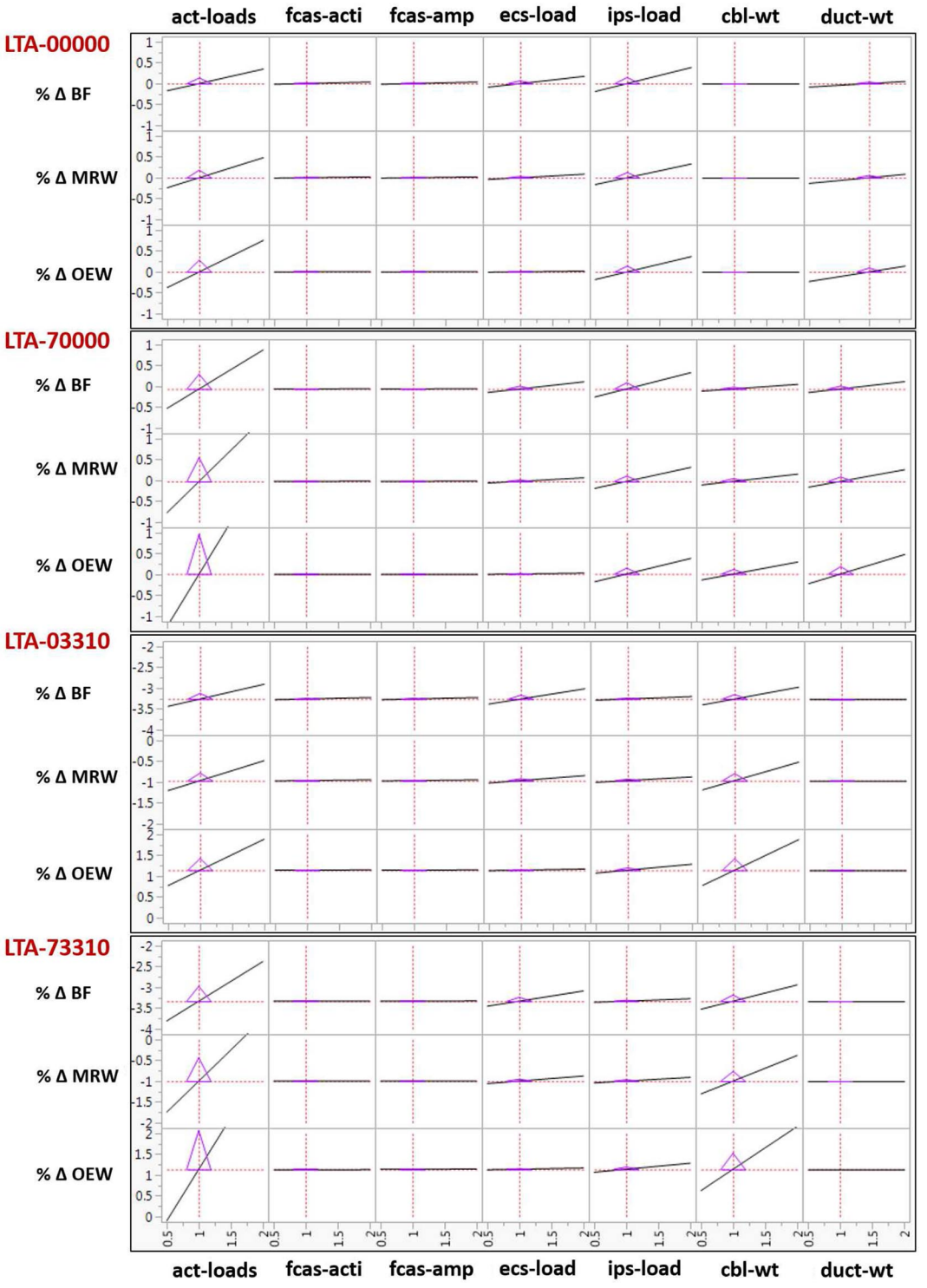

Fig. B3 Impact of individual epistemic uncertainty K-factors on performance of LTA-00000, LTA-70000, LTA-03310, and LTA-73310.

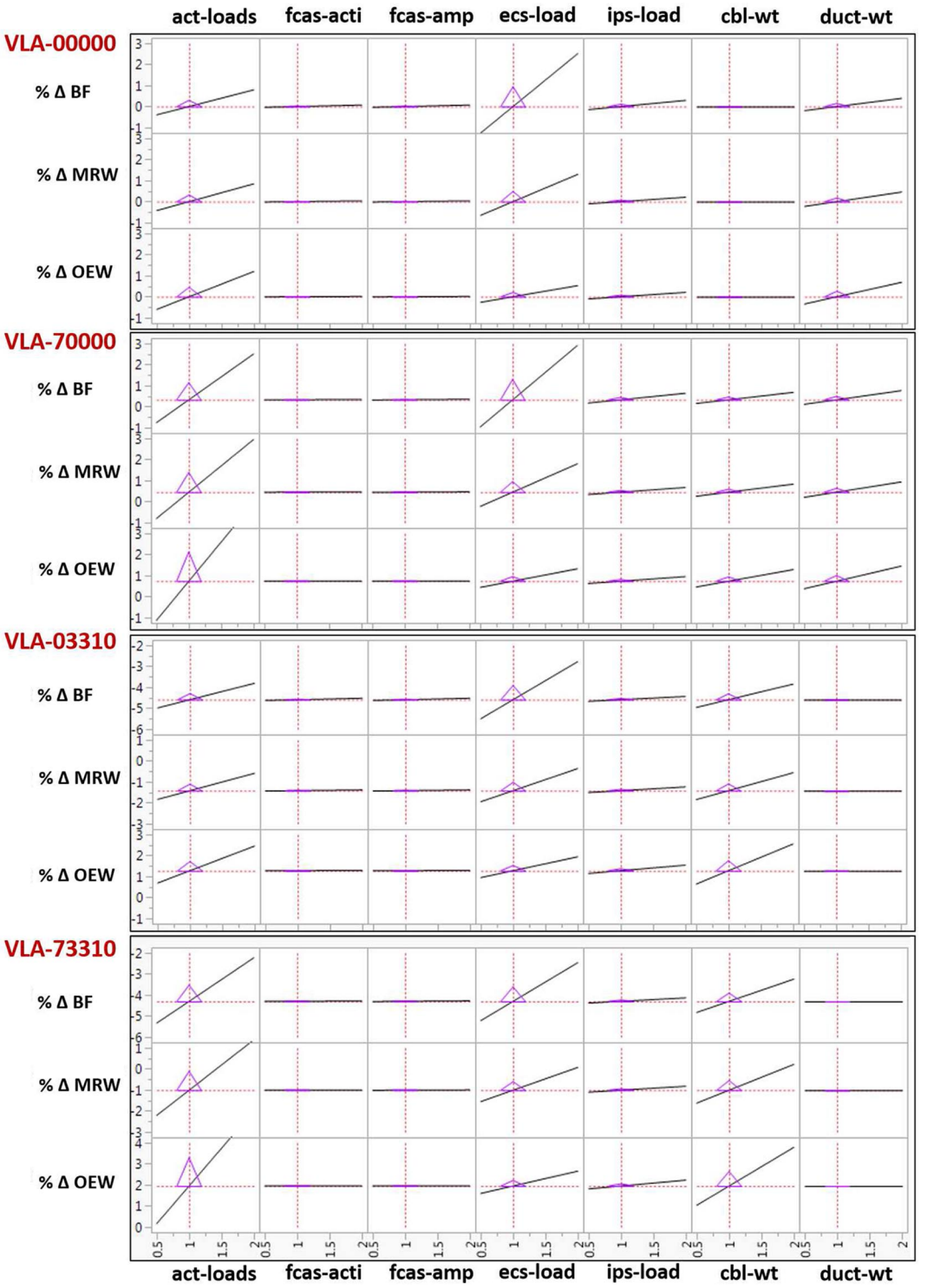

Fig. B4 Impact of individual epistemic uncertainty K-factors on performance of VLA-00000, VLA-70000, VLA-03310, and VLA-73310.

Appendix C: Sensitivity to Technological State-of-the-Art (LTA and VLA)

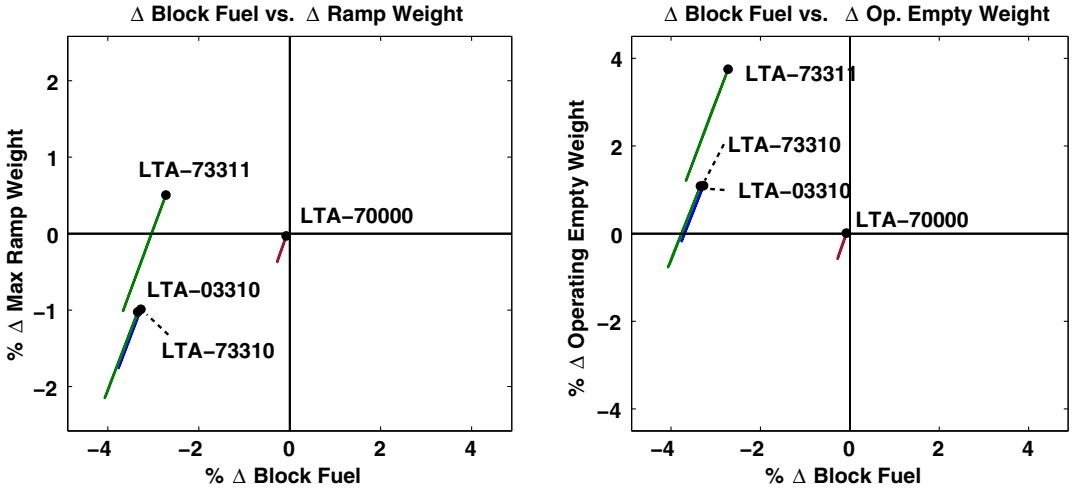

Fig. C1 Gross sensitivity of LTA-70000, LTA-03310, LTA-73310, and LTA-73311 to technological state-of-the-art.

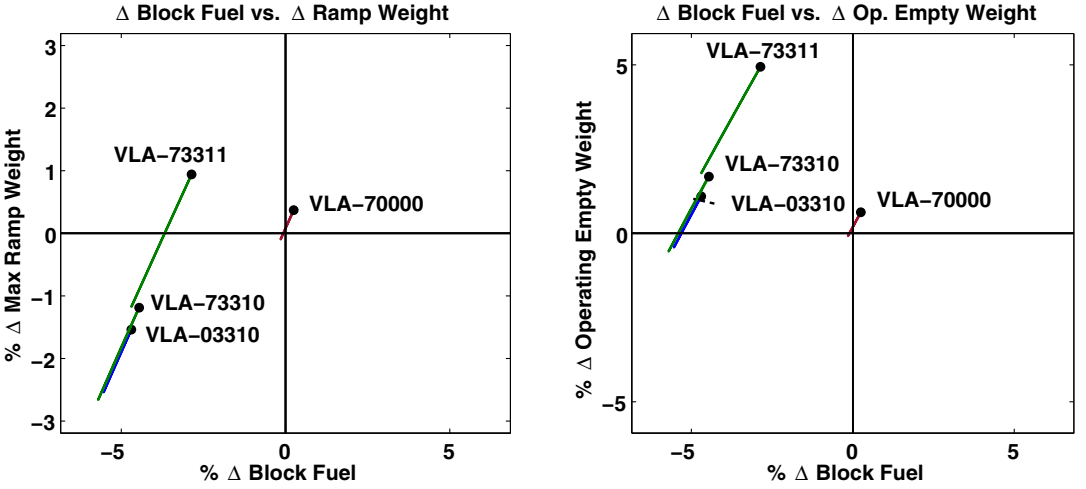

Fig. C2 Gross sensitivity of VLA-70000, VLA-03310, VLA-73310, and VLA-73311 to technological state-of-the-art.

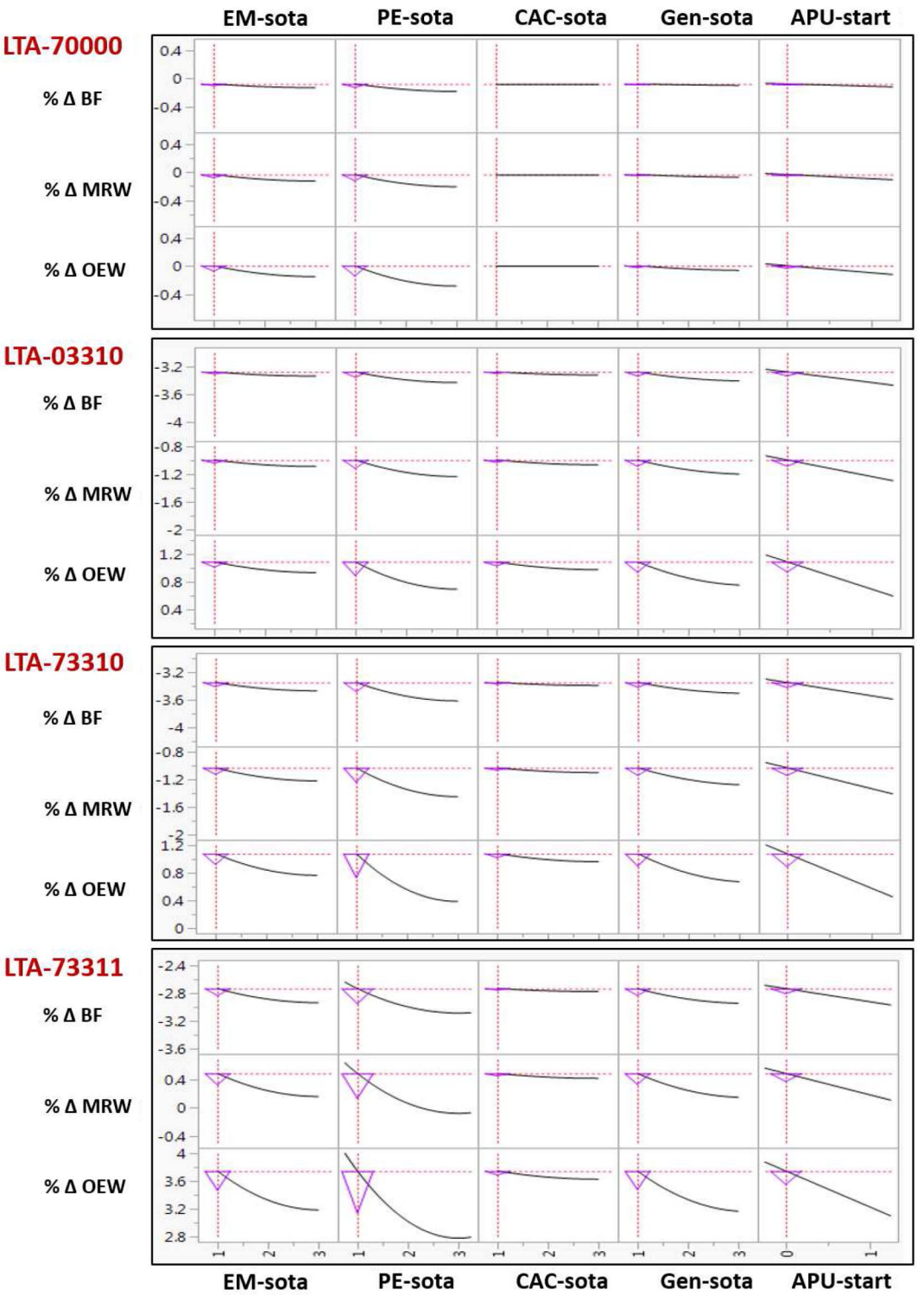

Fig. C3 Impact of individual technological SOTA K-factors on performance of LTA-70000, LTA-03310, LTA-73310, and LTA-73311.

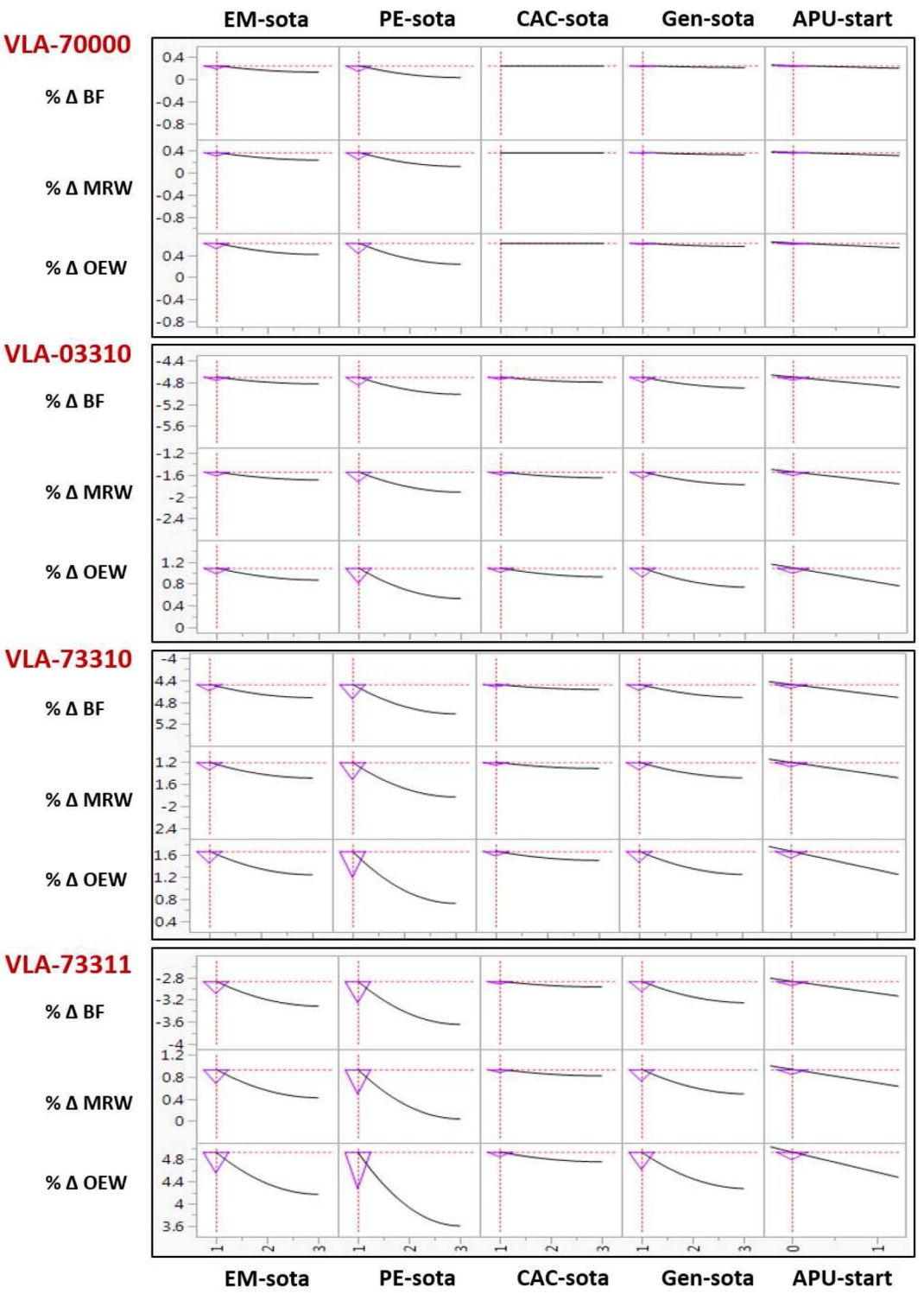

Fig. C4 Impact of individual technological SOTA K-factors on performance of VLA-70000, VLA-03310, VLA-73310, and VLA-73311.

References

[1] Faleiro, L., "Beyond the More Electric Aircraft," *AIAA Aerospace America*, Vol. 43, No. 9, Sept. 2005, pp. 35–40.

[2] Faleiro, L., Herzog, J., Schievelbusch, B., and Seung, T., "Integrated Equipment Systems for a More Electric Aircraft—Hydraulic and Pneumatics," *Proceedings of the 24th Congress of International Council of the Aeronautical Sciences*, ICAS Paper 2004-7.4.2, Yokohama, Japan, Sept. 2004.

[3] Jones, R., "The More Electric Aircraft—Assessing the Benefits," *Proceedings of the Institution of Mechanical Engineers, Part G: Journal of Aerospace Engineering*, Vol. 216, No. 5, 2002, pp. 259–269. doi:10.1243/095441002321028775

[4] Cronin, M., "The All-Electric Aircraft," *IEE Review*, Vol. 36, No. 8, Sept. 1990, pp. 309–311. doi:10.1049/ir:19900132

[5] Van den Bossche, D., "The A380 Flight Control Electrohydrostatic Actuators, Achievements and Lessons Learnt," *Proceedings of the 25th International Congress of the Aeronautical Sciences*, ICAS Paper 2006-7.4.1, Hamburg, Germany, Sept. 2006.

[6] Sinnett, M., "Boeing 787 No-Bleed Systems: Saving Fuel and Enhancing Operational Efficiencies," Boeing Aero Magazine, Quarter 4, 2007, http://www.boeing.com/commercial/aeromagazine [retrieved 24 April 2016].

[7] Chakraborty, I., "Subsystem Architecture Sizing and Analysis for Aircraft Conceptual Design," Ph.D. Dissertation, Daniel F. Guggenheim School of Aerospace Engineering, Georgia Inst. of Technology, Atlanta, GA, Dec. 2015, https://smartech.gatech.edu/handle/1853/54427 [retrieved 24 April 2016].

[8] Chakraborty, I., and Mavris, D., "Integrated Assessment of Aircraft and Novel Subsystem Architectures in Early Design," *54th AIAA Aerospace Sciences Meeting*, AIAA Paper 2016-0215, Jan. 2016.

[9] McCullers, L., "Flight Optimization System, Release 8.11, User's Guide," NASA Rept. 23681-0001, Oct. 2009.

[10] Lytle, J. K., "The Numerical Propulsion System Simulation: An Overview," NASA TM-2000-209915, June 2000, http://ntrs.nasa.gov/archive/nasa/casi.ntrs.nasa.gov/20000063377.pdf [retrieved 24 April 2016].

[11] Chakraborty, I., and Mavris, D., "Heuristic Definition, Evaluation, and Impact Decomposition of Aircraft Subsystem Architectures," *16th AIAA Aviation Technology, Integration, and Operations Conference*, AIAA Paper 2016-3144, June 2016.

[12] Roskam, J., *Airplane Design Part VI—Preliminary Calculation of Aerodynamic, Thrust and Power Characteristics, Design Analysis & Research Corporation*, Lawrence, KS, 1999.

[13] Scholz, D., "Development of a CAE-Tool for the Design of Flight Control and Hydraulic Systems," *AeroTech '95*, IMechE-Paper C505/9/011, Inst. of Mechanical Engineers, London, Oct. 1995.

[14] "Federal Aviation Regulations (FAR) Part 25—Airworthiness Standards: Transport Category Airplanes," Federal Aviation Administration, Washington, D.C., http://www.ecfr.gov [retrieved Nov. 2015].

[15] Simsic, C., "Electric Actuation System Duty Cycles," *Proceedings of the IEEE National Aerospace and Electronics Conference (NAECON 1991)*, Vol. 2, Inst. of Electrical and Electronics Engineers (IEEE), New York, 1991, pp. 540–545.

[16] Rudolph, P., "High Lift Systems on Subsonic Commercial Airliners," NASA CR-4746, Sept. 1996.

[17] "Flight Controls," *Boeing 777 Aircraft Maintenance Manual*, Boeing Airplane Company, Seattle, WA, 2006, Chap. 27.

[18] "Commercial Aircraft Hydraulic Systems," Society of Automotive Engineers, Aerospace Information Report (AIR), SAE International, Warrendale, PA, 2010.

[19] Lammering, T., "Integration of Aircraft Systems into Conceptual Design Synthesis," Ph.D. Dissertation, Inst. of Aeronautics and Astronautics, RWTH Aachen Univ., Aachen, Germany, 2014.

[20] Socheleau, J., Mare, J.-C., and Baudu, P., "Actuation Technologies and Application—Flight Controls and Thrust Reverser Actuation," *Technologies for Energy Optimized Aircraft Equipment Systems (TEOS Forum)*, Power Optimized Aircraft (POA) Project Consortium, Session 6A, Paris, 2006.

[21] Chakraborty, I., Mavris, D., Emeneth, M., and Schneegans, A., "An Integrated Approach to Vehicle and Subsystem Sizing and Analysis for Novel Subsystem Architectures," *Proceedings of the Institution of Mechanical Engineers, Part G: Journal of Aerospace Engineering*, Vol. 230, No. 3, 2016, pp. 496–514.

[22] Cameron-Johnson, A., "Some Aspects of the Design of Aircraft Steering Systems," *Aircraft Engineering and Aerospace Technology*, Vol. 43, No. 6, 1971, pp. 7–10. doi:10.1108/eb034778

[23] Bennett, J., Mecrow, B., Atkinson, D., Maxwell, C., and Benarous, M., "Fault-Tolerant Electric Drive for an Aircraft Nose Wheel Steering Actuator," *IET Electrical Systems in Transportation*, Vol. 1, No. 3, 2011, pp. 117–125. doi:10.1049/iet-est.2010.0054

[24] Collins, A., "EABSYS: Electrically Actuated Braking System," *Proceedings of the IEE Colloquium on Electrical Machines and Systems for the More Electric Aircraft*, The Inst. of Engineering and Technology (IET), London, 1999, p. 4.

[25] Scholz, D., "MPC 75 Hydraulic Load Analysis," Deutsche Airbus, TN-EV52-362/91, Hamburg, Germany, July 1991.

[26] Nicolas, Y., "eTaxi—Taxiing Aircraft with Engines Stopped," Flight Airworthiness Support Technology (FAST) 51, Airbus Technical Magazine, Jan. 2013, http://www.airbus.com/support/publications [retrieved 24 April 2016].

[27] Chakraborty, I., LeVine, M., and Hassan, M., "Assessing Taxiing Trade Spaces from Aircraft, Airport, and Airline Perspectives," *15th AIAA Aviation Technology, Integration, and Operations Conference*, AIAA Paper 2015-2386, June 2015.

[28] Herzog, J., "Electrification of the Environmental Control System," *Proceedings of the 25th International Congress of the Aeronautical Sciences*, ICAS Paper 2006-7.7.1, Hamburg, Germany, Sept. 2006.

[29] Meier, O., and Scholz, D., "A Handbook Method for the Estimation of Power Requirements for Electrical De-Icing Systems," *Proceedings of the Deutscher Luft- und Raumfahrtkongress 2010*, Hamburg, Germany, Aug.–Sept. 2010.

[30] Raymer, D., *Aircraft Design: A Conceptual Approach*, 4th ed., AIAA Education Series, AIAA, Reston, VA, 2006.

[31] Currey, N., *Aircraft Landing Gear Design: Principles and Practices*, AIAA Education Series, AIAA, Washington, D.C., 1988.

[32] Young, D., "Aircraft Landing Gears—The Past, Present and Future," *Proceedings of the Institution of Mechanical Engineers, Part D: Journal of Automobile Engineering*, Vol. 200, No. 24, 1986, pp. 75–92. doi:10.1243/PIME_PROC_1986_200_168_02

[33] Dodds, G., and Faleiro, L., "Technology for Energy Optimized Aircraft Equipment Systems—The Way Forward," *Technologies for Energy Optimized Aircraft Equipment Systems (TEOS Forum)*, Power Optimized Aircraft (POA) Project Consortium, 2006.

[34] Blanding, D., Sexton, M., Segal, M., and Grow, J., "The Application of Confidence Interval in the Evaluation of Electric Actuation Duty Cycle," *Proceedings of the 27th Congress of International Council of the Aeronautical Sciences*, ICAS Paper 2010-7.3.3, Nice, France, Sept. 2010.

[35] Wheeler, P. W., Clare, J. C., Trentin, A., and Bozhko, S., "An Overview of the More Electrical Aircraft," *Proceedings of the Institution of Mechanical Engineers, Part G: Journal of Aerospace Engineering*, Vol. 227, No. 4, 2012, pp. 578–585. doi:10.1177/0954410012468538

[36] Chakraborty, I., Trawick, D., Jackson, D., and Mavris, D., "Electric Control Surface Actuator Design Optimization and Allocation for the More Electric Aircraft," *2013 Aviation Technology, Integration, and Operations Conference*, AIAA Paper 2013-4283, Aug. 2013.

[37] Rea, J., "Boeing 777 High Lift Control System," *IEEE Aerospace and Electronic Systems Magazine*, Vol. 8, No. 8, Aug. 1993, pp. 15–21. doi:10.1109/62.248331

[38] "Aerospace Capabilities—Boeing 777," Eaton Aerospace Group, Irvine, CA, April 2014, http://www.eaton.com/ecm/groups/public/@pub/@eaton/@aero/documents/content/ct_194202.pdf [retrieved Nov. 2015].

[39] Martinez, M., Sawata, T., Rouge-Carrassat, T., and Blineau, J.-M., "Electrical Power Sources and Aircraft Power Networks," *Technologies for Energy Optimized Aircraft Equipment Systems (TEOS Forum)*, Power Optimized Aircraft (POA) Project Consortium, Session 2C, Paris, 2006.

[40] Slingerland, R., Zandstra, S., Scholz, D., and Seeckt, K., "Green Freighter Systems," *46th AIAA Aerospace Sciences Meeting and Exhibit*, AIAA Paper 2008-0146, Jan. 2008.

[41] Xia, X., "Dynamic Power Distribution Management for All Electric Aircraft," M.S. Thesis, School of Engineering, Cranfield Univ., Cranfield, England, U.K., 2011.